Acta Cryst E CRYSTALLOGRAPHIC COMMUNICATIONS

ISSN 2056-9890

Synthesis and crystal structure of ABW-type $SrFe_{1.40}V_{0.60}O_4$

Thomas Gstir,[a] Volker Kahlenberg,[a]* Hannes Krüger[a] and Simon Penner[b]

[a]University of Innsbruck, Institute of Mineralogy & Petrography, Innrain 52, A-6020 Innsbruck, Austria, and [b]University of Innsbruck, Department of Physical Chemistry, Innrain 52c, A-6020 Innsbruck, Austria. *Correspondence e-mail: volker.kahlenberg@uibk.ac.at

Received 30 March 2020
Accepted 8 April 2020

Edited by M. Weil, Vienna University of Technology, Austria

Keywords: crystal structure; cation substitution; solid solution; topology; zeolite; ABW.

CCDC reference: 1995764

Supporting information: this article has supporting information at journals.iucr.org/e

Single crystals of $SrFe_{1.40}V_{0.60}O_4$, strontium tetraoxidodi[ferrate(III)/vanadate(III)], have been obtained as a side product in the course of sinter experiments aimed at the synthesis of double perovskites in the system SrO–Fe_2O_3–V_2O_5. The crystal structure can be characterized by layers of six-membered rings of TO_4-tetrahedra (T: Fe^{III}, V^{III}) perpendicular to [100]. Stacking of the layers along [100] results in a three-dimensional framework enclosing tunnel-like cavities in which Sr^{II} cations are incorporated for charge compensation. The sequence of directedness of up (U) and down (D) pointing vertices of neighboring tetrahedra in a single six-membered ring is $UUUDDD$. The topology of the tetrahedral framework belongs to the zeolite-type ABW.

1. Chemical context

Solid oxide fuel cell (SOFC) technology is considered as particularly promising for energy storage applications (Larminie *et al.*, 2003). SOFCs are electrochemical devices that consist of three main parts: (i) a redox-capable porous cathode that reduces O_2 to O^{2-} anions, (ii) an electrolyte transporting these anions to the anode, and (iii) the anode, where the fuel (hydrogen or carbon-containing fuels) is electro-oxidized by the O^{2-} anions to CO_2 and H_2O (Huang & Goodenough, 2009). Double perovskites with the general composition $A_2(BB')O_6$ have been studied intensively as potential anode materials in SOFCs (Xu *et al.*, 2019). In the course of an explorative study on double perovskites combining mixed ionic-electronic conductivity with catalytic activity for fuel oxidation, we tried to synthesize Sr_2FeVO_6 using a ceramic synthesis route in the range between 1473 and 1573 K. For the highest reaction temperature, where partial melting occurred, a member of the previously unknown $SrFe_xV_{2-x}O_4$ solid-solution series was observed as a side-product, and the crystal structure of the member with x = 1.40 is reported here.

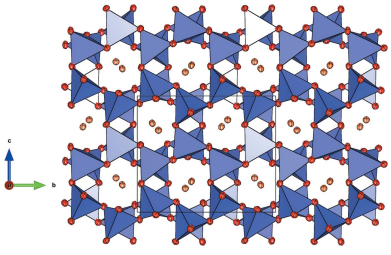

2. Structural commentary

$SrFe_{1.40}V_{0.60}O_4$ exhibits a three-dimensional framework of corner-linked TO_4-tetrahedra (T: Fe^{III}, V^{III}). Charge compensation is achieved by the incorporation of Sr^{II} cations residing in tunnel-like cavities running parallel to [100] (Fig. 1). The compound is isostructural with $SrFe_2O_4$ (Kahlenberg & Fischer, 2001) and γ-$SrGa_2O_4$ (Kahlenberg *et al.*, 2000).

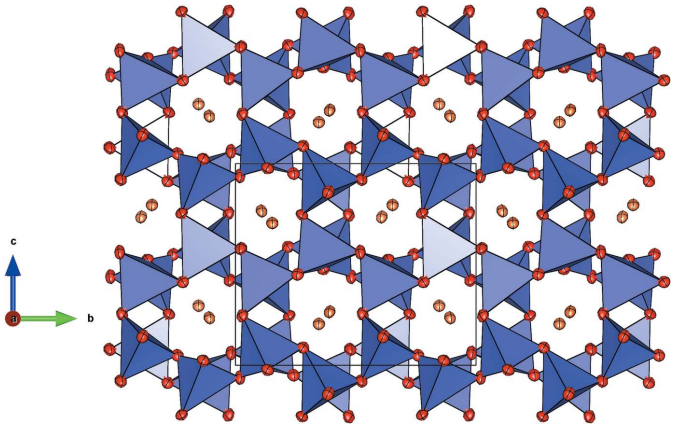

Figure 1
Projection of the framework structure along [100]. [TO_4] tetrahedra are shown in blue. Oxygen and strontium atoms are given in red and orange, respectively. Displacement ellipsoids are drawn at the 70% probability level.

All atoms occupy general positions. Fe <—> V substitutions occur on each of the four symmetrically non-equivalent *T*-sites occupying the centers of distorted tetrahedra formed by oxygen atoms. Site-population refinements indicate no clear trend when comparing the individual Fe:V distributions. The Fe:V population at the *T*-sites is more or less balanced ranging from 64 (3) to 75 (3)% of iron. Individual *T*—O distances adopt values between 1.820 (6) and 1.901 (5) Å. The distortion of the tetrahedra is also reflected in the variation of the O—*T*—O bond angles scattering between 98.2 (2) and 129.9 (2)°. According to Robinson *et al.* (1971), the distortions can be expressed numerically by means of the quadratic elongation λ and the angle variance σ^2. These two parameters exhibit values between 1.009 and 1.016 for λ and 34.72 and 59.96 for σ^2.

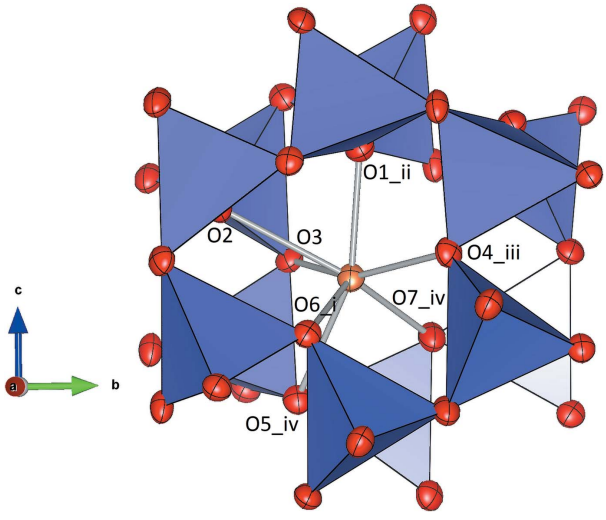

Figure 2
Representation of the coordination polyhedron around Sr1. Displacement ellipsoids are drawn at the 70% probability level. [Symmetry codes: (i) $1-x, 1-y, 1-z$; (ii) $\frac{1}{2}+x, \frac{1}{2}-y, -\frac{1}{2}+z$; (iii) $\frac{3}{2}-x, \frac{1}{2}+y, \frac{1}{2}-z$; (iv) $-\frac{1}{2}+x, \frac{1}{2}-y, -\frac{1}{2}+z$].

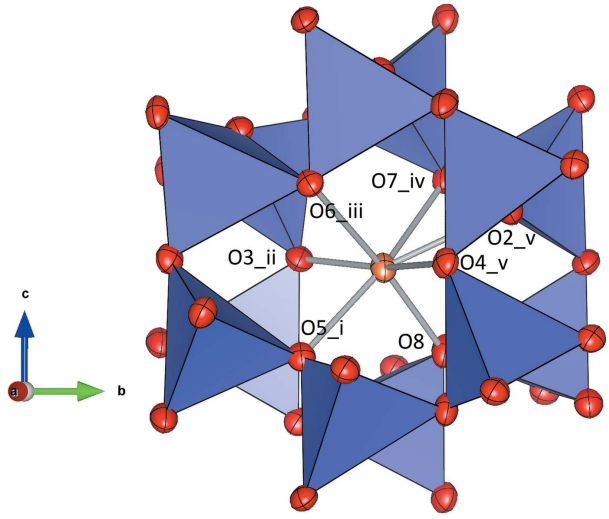

Figure 3
Representation of the coordination polyhedron around Sr2. Ellipsoids are drawn at the 70% level. [Symmetry codes: (i) $\frac{3}{2}-x, \frac{1}{2}+y, \frac{1}{2}-z$; (ii) $\frac{1}{2}-x, \frac{1}{2}+y, \frac{1}{2}-z$; (iii) $\frac{1}{2}+x, \frac{3}{2}-y, -\frac{1}{2}+z$; (iv) $1-x, 1-y, 1-z$; (v) $x, 1+y, z$]

Each of the two symmetrically independent Sr^{II} cations is coordinated by seven oxygen atoms within the channels of the framework. They are located off-center and have irregular coordination spheres formed by the oxygen atoms of two adjacent six-membered tetrahedral rings (Figs. 2, 3). Bond-valence-sum calculations using the parameter sets for the Sr—O bonds given by Brown & Altermatt (1985) resulted in the following values (in v.u.) considering cation–anion interactions up to 3.2 Å: Sr1: 1.911 and Sr2: 1.692. The considerable underbonding of the Sr2 position indicates that the bonds are stretched and that this Sr site resides in a cavity that is too large. A similar situation has been observed in isostructural $SrFe_2O_4$ and γ-$SrGa_2O_4$.

3. Topological features

$SrFe_{1.40}V_{0.60}O_4$ belongs to the ABW zeolite structure type (Baerlocher *et al.*, 2007). This class of materials comprises a large number of representatives and has been investigated in great detail because of the complex phase transitions and interesting ferroic effects (Bu *et al.*, 1997). The polyhedral connectivity results in a three-dimensional network built from six-, four- and eight-membered rings. Perpendicular to [100], for example, the structure can be decomposed into layers consisting of six-membered rings (S6R) of [TO_4]-tetrahedra forming honeycomb nets (Fig. 4). Within a single S6R, three tetrahedra with vertices up (*U*) alternate with three tetrahedra having their vertices down (*D*) (sequence of directedness: *UUUDDD*). Using the terminology of Flörke (1967), the relative orientation of paired tetrahedra belonging to different adjacent layers can be approximately classified as a *trans*-configuration (Fig. 1). Alternatively, the layers can be regarded as being constructed from the condensation of unbranched *vierer* single-chains *via* common corners.

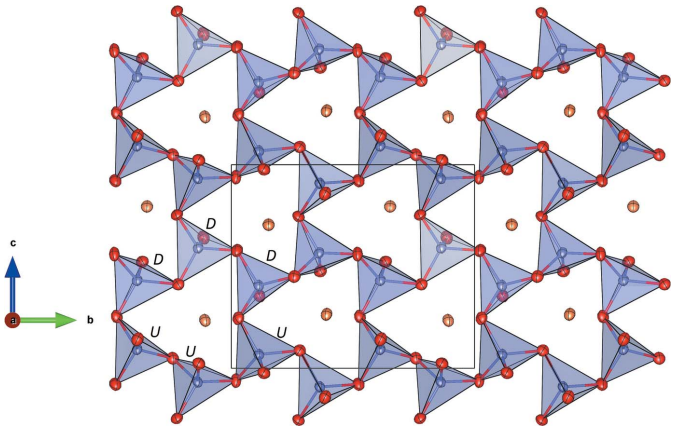

Figure 4
Single tetrahedral layer with six-membered rings in a projection along [100]. *T*-sites in the centres of the tetrahedra are shown in blue. Displacement ellipsoids are drawn at the 70% probability level.

Perpendicular to [010] the network contains strongly corrugated layers of S4R and S8R (Fig. 5). The S8Rs are highly elliptical. Subsequent layers are connected by bridging vertex oxygen atoms, forming eight-ring channels that propagate along [010]. The elliptical shape of the channels is also reflected in the high framework density (Brunner & Meyer, 1989), with a value of 20.0 tetrahedral atoms/1000 Å^3.

Table 1
Experimental details.

Crystal data	
Chemical formula	$SrFe_{1.40}V_{0.60}O_4$
M_r	260.37
Crystal system, space group	Monoclinic, $P2_1/n$
Temperature (K)	100
a, b, c (Å)	8.0594 (8), 10.8768 (9), 9.1218 (8)
β (°)	91.544 (7)
V (Å^3)	799.33 (12)
Z	8
Radiation type	Synchrotron, λ = 0.72931 Å
μ (mm^{-1})	20.91
Crystal size (mm)	0.03 × 0.02 × 0.01
Data collection	
Diffractometer	Aerotech
Absorption correction	Multi-scan (*CrysAlis PRO*; Rigaku OD, 2018)
T_{min}, T_{max}	0.614, 0.871
No. of measured, independent and observed [$I > 2\sigma(I)$] reflections	5200, 1746, 1572
R_{int}	0.067
(sin $\theta/\lambda)_{max}$ (Å^{-1})	0.641
Refinement	
$R[F^2 > 2\sigma(F^2)]$, $wR(F^2)$, S	0.050, 0.144, 1.14
No. of reflections	1746
No. of parameters	131
$\Delta\rho_{max}$, $\Delta\rho_{min}$ (e Å^{-3})	1.74, −1.37

Computer programs: *CrysAlis PRO* (Rigaku OD, 2018), *SHELXL97* (Sheldrick, 2008), *VESTA* (Momma & Izumi, 2011), *publCIF* (Westrip, 2010) and *WinGX* (Farrugia, 2012).

4. Synthesis and initial characterization

Single-crystals of $SrFe_{1.40}V_{0.60}O_4$ were obtained in the course of a series of synthesis experiments aimed at the preparation of a possible double perovskite phase with composition Sr_2FeVO_6. Therefore, mixtures of the dried starting materials $SrCO_3$, Fe_2O_3 and V_2O_5 were homogenized in the molar ratio 4:1:1 using a ball mill operated at 600 r.p.m. for 45 min under ethanol. The resulting slurry was dried for 24 h at 323 K and subsequently re-ground by hand. An amount of about 0.5 g was pressed into a pellet having a diameter of 12 mm. Thermal treatment was performed in a resistance-heated horizontal tube furnace in air. Therefore, the tablet was placed on a platinum foil contained in an alumina-ceramic combustion boat. The sample was heated from 298 K to 1473 K with a ramp of 100 K h^{-1}, followed by 25 K h^{-1} to 1423 K and finally at 10 h K^{-1} to 1573 K. After annealing for 48 h at the maximum temperature, the container was quenched to room temperature. The partially melted pellet was removed from the foil, crushed in an agate mortar and transferred to a glass slide under a reflected-light microscope. A first optical inspection revealed the presence of at least two different crystalline phases: (*a*) larger, transparent–colorless crystals up to 150 µm in size and (*b*) considerably smaller, opaque black–brown specimens with maximum dimensions of about 50 µm. Preliminary single-crystal diffraction experiments revealed the larger crystals to be $Sr_3(VO_4)_2$ (Carrillo-Cabrera & von Schnering, 1993) while the second phase could be indexed with a monoclinic primitive unit cell similar to the one reported for $SrFe_2O_4$ (Kahlenberg & Fischer, 2001). Since the larger samples of the second phase always exhibited intergrowth of several crystals, we finally decided to focus on the fraction with smaller crystallites and to perform the relevant diffraction studies for structure elucidation using synchrotron radiation at the X06DA beamline of the Swiss Light Source, Paul Scherrer Institute, Villigen, Switzerland. Therefore, a sample was mounted on the tip of a 0.25 mm diameter LithoLoop made by Molecular Dimensions Inc. with a drop of Paratone-N oil (Hampton Research) and flash cooled in a 100 K nitrogen gas stream.

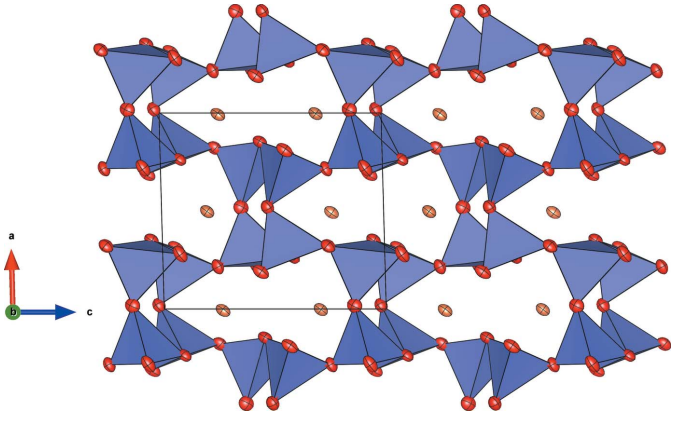

Figure 5
Strongly folded tetrahedral layer with four- and eight-membered rings in a projection along [010]. Displacement ellipsoids are drawn at the 70% probability level.

5. Refinement

Crystal data, data collection and structure refinement details are summarized in Table 1. Initial coordinates for the refinement calculations were taken from the crystal structure refinement of $SrFe_2O_4$ (Kahlenberg & Fischer, 2001) after transformation to monoclinic second setting. Site-population refinements of the Fe:V ratios on the *T*-sites indicated the presence of a member of the solid-solution series $SrFe_xV_{2-x}O_4$.

Acknowledgements

Anuschka Pauluhn is thanked for her help during the data collections at the X06DA beamline. The research leading to these results has received funding from the European Union's Horizon 2020 research and innovation programme under grant agreement No. 730872, project CALIPSOplus.

References

Baerlocher, Ch., McCusker, L. B. & Olson, D. H. (2007). *Atlas of Zeolite Framework Types*, 6th revised ed. Amsterdam: Elsevier.
Brown, I. D. & Altermatt, D. (1985). *Acta Cryst.* B**41**, 244–247.
Brunner, G. O. & Meyer, W. M. (1989). *Nature*, **337**, 146–147.
Bu, X., Feng, P., Gier, T. E. & Stucky, G. D. (1997). *Zeolites*, **19**, 200–208.
Carrillo-Cabrera, W. & von Schnering, H. G. (1993). *Z. Kristallogr.* **205**, 271–276.
Farrugia, L. J. (2012). *J. Appl. Cryst.* **45**, 849–854.
Flörke, O. (1967). *Fortschr. Mineral*, **44**, 181–230.
Huang, K. & Goodenough, J. B. (2009). *Solid Oxide Fuel Cell Technology: Principles, Performance and Operations*. New York: Woodhead Publishing in Energy, CRC Press.
Kahlenberg, V. & Fischer, R. X. (2001). *Solid State Sci.* **3**, 433–439.
Kahlenberg, V., Fischer, R. X. & Shaw, C. S. J. (2000). *J. Solid State Chem.* **153**, 294–300.
Larminie, J., Dicks, A. & McDonald, M. S. (2003). *Fuel cells explained.* Vol. 2. New York: Wiley.
Momma, K. & Izumi, F. (2011). *J. Appl. Cryst.* **44**, 1272–1276.
Rigaku OD (2018). *CrysAlis PRO*. Rigaku Oxford Diffraction, Yarnton, England.
Robinson, K., Gibbs, G. V. & Ribbe, P. H. (1971). *Science*, **172**, 567–570.
Sheldrick, G. M. (2008). *Acta Cryst.* A**64**, 112–122.
Westrip, S. P. (2010). *J. Appl. Cryst.* **43**, 920–925.
Xu, X., Zhong, Y. & Shao, Z. (2019). *Trends Chem.* **1**, 410–424.

supporting information

Acta Cryst. (2020). E**76**, 664-667 [https://doi.org/10.1107/S205698902000496X]

Synthesis and crystal structure of ABW-type $SrFe_{1.40}V_{0.60}O_4$

Thomas Gstir, Volker Kahlenberg, Hannes Krüger and Simon Penner

Computing details

Data collection: *CrysAlis PRO* (Rigaku OD, 2018); cell refinement: *CrysAlis PRO* (Rigaku OD, 2018); data reduction: *CrysAlis PRO* (Rigaku OD, 2018); program(s) used to refine structure: *SHELXL97* (Sheldrick, 2008); molecular graphics: *VESTA* (Momma & Izumi, 2011); software used to prepare material for publication: *publCIF* (Westrip, 2010) and *WinGX* (Farrugia, 2012).

Strontium tetraoxidodi[ferrate(III)/vanadate(III)]

Crystal data

$SrFe_{1.40}V_{0.60}O_4$
M_r = 260.37
Monoclinic, $P2_1/n$
Hall symbol: -P 2yn
a = 8.0594 (8) Å
b = 10.8768 (9) Å
c = 9.1218 (8) Å
β = 91.544 (7)°
V = 799.33 (12) Å^3
Z = 8
$F(000)$ = 961.6
D_x = 4.327 Mg m^{-3}
Synchrotron radiation, λ = 0.72931 Å
Cell parameters from 2398 reflections
θ = 3.5–33.9°
μ = 20.91 mm^{-1}
T = 100 K
Fragment, brown-black
0.03 × 0.02 × 0.01 mm

Data collection

Aerotech diffractometer
Radiation source: SLS super-bending magnet 2.9T, X06DA
Bartels Monochromator with dual channel cut crystals (DCCM) in (±∓) geometry monochromator
Detector resolution: 5.81 pixels mm^{-1}
rotation method scans
Absorption correction: multi-scan (*CrysAlis PRO*; Rigaku OD, 2018)
T_{min} = 0.614, T_{max} = 0.871
5200 measured reflections
1746 independent reflections
1572 reflections with $I > 2\sigma(I)$
R_{int} = 0.067
θ_{max} = 27.9°, θ_{min} = 3.0°
h = −9→10
k = −13→13
l = −11→11

Refinement

Refinement on F^2
Least-squares matrix: full
$R[F^2 > 2\sigma(F^2)]$ = 0.050
$wR(F^2)$ = 0.144
S = 1.14
1746 reflections
131 parameters
0 restraints
Primary atom site location: isomorphous structure methods
Secondary atom site location: notdet
$w = 1/[\sigma^2(F_o^2) + (0.0821P)^2]$ where $P = (F_o^2 + 2F_c^2)/3$
$(\Delta/\sigma)_{max} < 0.001$
$\Delta\rho_{max}$ = 1.74 e Å^{-3}
$\Delta\rho_{min}$ = −1.37 e Å^{-3}

Special details

Geometry. All esds (except the esd in the dihedral angle between two l.s. planes) are estimated using the full covariance matrix. The cell esds are taken into account individually in the estimation of esds in distances, angles and torsion angles; correlations between esds in cell parameters are only used when they are defined by crystal symmetry. An approximate (isotropic) treatment of cell esds is used for estimating esds involving l.s. planes.

Refinement. Refinement of F^2 against ALL reflections. The weighted R-factor wR and goodness of fit S are based on F^2, conventional R-factors R are based on F, with F set to zero for negative F^2. The threshold expression of $F^2 > 2\sigma(F^2)$ is used only for calculating R-factors(gt) etc. and is not relevant to the choice of reflections for refinement. R-factors based on F^2 are statistically about twice as large as those based on F, and R- factors based on ALL data will be even larger.

Fractional atomic coordinates and isotropic or equivalent isotropic displacement parameters (Å²)

	x	*y*	*z*	U_{iso}*/U_{eq}	Occ. (<1)
Sr1	0.49713 (9)	0.34684 (7)	0.20513 (7)	0.0190 (3)	
Sr2	0.50716 (9)	0.89165 (6)	0.23511 (8)	0.0193 (3)	
Fe1	0.22326 (15)	0.13896 (10)	0.06706 (12)	0.0163 (4)	0.64 (3)
Fe2	0.29893 (14)	0.13638 (10)	0.40844 (12)	0.0164 (4)	0.75 (3)
Fe3	0.17887 (15)	0.88717 (9)	0.93230 (12)	0.0166 (4)	0.71 (4)
Fe4	0.74301 (15)	0.11238 (9)	0.40681 (12)	0.0159 (4)	0.70 (3)
V1	0.22326 (15)	0.13896 (10)	0.06706 (12)	0.0163 (4)	0.36 (3)
V2	0.29893 (14)	0.13638 (10)	0.40844 (12)	0.0164 (4)	0.25 (3)
V3	0.17887 (15)	0.88717 (9)	0.93230 (12)	0.0166 (4)	0.29 (4)
V4	0.74301 (15)	0.11238 (9)	0.40681 (12)	0.0159 (4)	0.30 (3)
O1	0.0192 (7)	0.1337 (5)	0.9770 (6)	0.0218 (11)	
O2	0.5181 (7)	0.1144 (5)	0.3576 (6)	0.0235 (12)	
O3	0.2158 (6)	0.2238 (5)	0.2460 (5)	0.0208 (11)	
O4	0.8217 (6)	0.0290 (5)	0.2457 (5)	0.0209 (11)	
O5	0.8530 (6)	0.2590 (5)	0.4510 (5)	0.0196 (10)	
O6	0.2367 (6)	0.7187 (5)	0.9126 (5)	0.0193 (11)	
O7	0.7805 (7)	0.0230 (5)	0.5784 (5)	0.0238 (12)	
O8	0.3105 (6)	0.9810 (5)	0.0607 (6)	0.0217 (11)	

Atomic displacement parameters (Å²)

	U^{11}	U^{22}	U^{33}	U^{12}	U^{13}	U^{23}
Sr1	0.0171 (4)	0.0186 (4)	0.0210 (4)	−0.0003 (3)	−0.0052 (3)	0.0001 (2)
Sr2	0.0184 (5)	0.0167 (4)	0.0226 (4)	0.0007 (2)	−0.0058 (3)	−0.0016 (2)
Fe1	0.0162 (7)	0.0141 (6)	0.0182 (6)	−0.0007 (4)	−0.0042 (4)	−0.0008 (4)
Fe2	0.0161 (7)	0.0146 (6)	0.0183 (6)	0.0005 (4)	−0.0038 (4)	0.0007 (4)
Fe3	0.0163 (7)	0.0148 (7)	0.0184 (6)	−0.0006 (4)	−0.0051 (4)	−0.0002 (4)
Fe4	0.0154 (7)	0.0140 (6)	0.0182 (6)	−0.0002 (4)	−0.0047 (4)	−0.0005 (4)
V1	0.0162 (7)	0.0141 (6)	0.0182 (6)	−0.0007 (4)	−0.0042 (4)	−0.0008 (4)
V2	0.0161 (7)	0.0146 (6)	0.0183 (6)	0.0005 (4)	−0.0038 (4)	0.0007 (4)
V3	0.0163 (7)	0.0148 (7)	0.0184 (6)	−0.0006 (4)	−0.0051 (4)	−0.0002 (4)
V4	0.0154 (7)	0.0140 (6)	0.0182 (6)	−0.0002 (4)	−0.0047 (4)	−0.0005 (4)
O1	0.024 (3)	0.022 (3)	0.019 (3)	−0.003 (2)	−0.002 (2)	−0.001 (2)
O2	0.024 (3)	0.020 (3)	0.027 (3)	0.002 (2)	−0.002 (2)	−0.004 (2)
O3	0.025 (3)	0.018 (3)	0.019 (2)	0.001 (2)	−0.0046 (19)	0.0019 (19)
O4	0.022 (3)	0.018 (3)	0.023 (2)	0.005 (2)	−0.003 (2)	0.002 (2)

O5	0.018 (3)	0.019 (2)	0.022 (2)	−0.001 (2)	−0.0044 (18)	0.001 (2)
O6	0.016 (3)	0.020 (3)	0.021 (2)	−0.002 (2)	−0.0041 (18)	0.0004 (19)
O7	0.031 (3)	0.018 (3)	0.022 (3)	−0.002 (2)	−0.009 (2)	0.0020 (19)
O8	0.021 (3)	0.015 (3)	0.028 (3)	0.000 (2)	−0.009 (2)	0.001 (2)

Geometric parameters (Å, º)

Sr1—O1^{i}	2.490 (5)	Fe4—O5	1.863 (5)
Sr1—O4^{ii}	2.495 (5)	O1—V1^{xiii}	1.820 (6)
Sr1—O7^{iii}	2.506 (5)	O1—Fe1^{xiii}	1.820 (6)
Sr1—O6^{iv}	2.527 (5)	O1—V3^{xii}	1.832 (6)
Sr1—O3	2.668 (5)	O1—Fe3^{xii}	1.832 (6)
Sr1—O5^{iii}	2.811 (5)	O1—Sr1^{xiv}	2.490 (5)
Sr1—O2	2.889 (5)	O2—Sr2^{ix}	2.668 (5)
Sr2—O8	2.419 (5)	O3—Sr2^{xv}	2.571 (5)
Sr2—O5^{ii}	2.517 (5)	O4—V3^{iv}	1.862 (5)
Sr2—O3^{v}	2.571 (5)	O4—Fe3^{iv}	1.862 (5)
Sr2—O2^{vi}	2.668 (5)	O4—Sr1^{xvi}	2.495 (5)
Sr2—O6^{vii}	2.706 (5)	O4—Sr2^{ix}	2.942 (5)
Sr2—O4^{vi}	2.942 (5)	O5—V1^{xvii}	1.872 (5)
Sr2—O7^{iv}	3.057 (6)	O5—Fe1^{xvii}	1.872 (5)
Fe1—O1^{viii}	1.820 (6)	O5—Sr2^{xvi}	2.517 (5)
Fe1—O8^{ix}	1.858 (5)	O5—Sr1^{xvii}	2.811 (5)
Fe1—O5^{iii}	1.872 (5)	O6—V2^{xviii}	1.891 (5)
Fe1—O3	1.877 (5)	O6—Fe2^{xviii}	1.891 (5)
Fe2—O7^{x}	1.853 (6)	O6—Sr1^{iv}	2.527 (5)
Fe2—O2	1.854 (6)	O6—Sr2^{xix}	2.706 (5)
Fe2—O3	1.869 (5)	O7—V2^{x}	1.853 (6)
Fe2—O6^{xi}	1.891 (5)	O7—Fe2^{x}	1.853 (6)
Fe3—O1^{xii}	1.832 (6)	O7—Sr1^{xvii}	2.506 (5)
Fe3—O4^{iv}	1.862 (5)	O7—Sr2^{iv}	3.057 (6)
Fe3—O8^{xiii}	1.863 (5)	O8—V1^{vi}	1.858 (5)
Fe3—O6	1.901 (5)	O8—Fe1^{vi}	1.858 (5)
Fe4—O4	1.853 (5)	O8—V3^{viii}	1.863 (5)
Fe4—O2	1.855 (6)	O8—Fe3^{viii}	1.863 (5)
Fe4—O7	1.860 (5)		

O1^{i}—Sr1—O4^{ii}	74.21 (17)	V1^{xiii}—O1—Fe3^{xii}	126.0 (3)
O1^{i}—Sr1—O7^{iii}	116.19 (18)	Fe1^{xiii}—O1—Fe3^{xii}	126.0 (3)
O4^{ii}—Sr1—O7^{iii}	91.79 (17)	V3^{xii}—O1—Fe3^{xii}	0.00 (7)
O1^{i}—Sr1—O6^{iv}	114.11 (17)	V1^{xiii}—O1—Sr1^{xiv}	119.1 (3)
O4^{ii}—Sr1—O6^{iv}	78.52 (16)	Fe1^{xiii}—O1—Sr1^{xiv}	119.1 (3)
O7^{iii}—Sr1—O6^{iv}	123.51 (17)	V3^{xii}—O1—Sr1^{xiv}	114.9 (3)
O1^{i}—Sr1—O3	86.65 (17)	Fe3^{xii}—O1—Sr1^{xiv}	114.9 (3)
O4^{ii}—Sr1—O3	150.33 (16)	Fe2—O2—Fe4	150.7 (3)
O7^{iii}—Sr1—O3	76.34 (16)	Fe2—O2—Sr2^{ix}	101.6 (2)
O6^{iv}—Sr1—O3	130.71 (16)	Fe4—O2—Sr2^{ix}	96.4 (2)
O1^{i}—Sr1—O5^{iii}	150.77 (17)	Fe2—O2—Sr1	87.9 (2)

O4^{ii}—Sr1—O5^{iii}	134.45 (15)	Fe4—O2—Sr1	99.8 (2)
O7^{iii}—Sr1—O5^{iii}	65.40 (15)	Sr2^{ix}—O2—Sr1	126.3 (2)
O6^{iv}—Sr1—O5^{iii}	82.57 (15)	Fe2—O3—Fe1	114.8 (3)
O3—Sr1—O5^{iii}	64.90 (14)	Fe2—O3—Sr2^{xv}	123.0 (2)
O1^{i}—Sr1—O2	66.00 (15)	Fe1—O3—Sr2^{xv}	116.5 (2)
O4^{ii}—Sr1—O2	125.61 (16)	Fe2—O3—Sr1	94.5 (2)
O7^{iii}—Sr1—O2	138.40 (18)	Fe1—O3—Sr1	94.5 (2)
O6^{iv}—Sr1—O2	85.32 (17)	Sr2^{xv}—O3—Sr1	104.54 (18)
O3—Sr1—O2	62.13 (16)	Fe4—O4—V3^{iv}	117.3 (3)
O5^{iii}—Sr1—O2	93.22 (15)	Fe4—O4—Fe3^{iv}	117.3 (3)
O8—Sr2—O5^{ii}	94.82 (17)	V3^{iv}—O4—Fe3^{iv}	0.00 (6)
O8—Sr2—O3^{v}	83.26 (16)	Fe4—O4—Sr1^{xvi}	117.2 (2)
O5^{ii}—Sr2—O3^{v}	87.97 (16)	V3^{iv}—O4—Sr1^{xvi}	122.2 (2)
O8—Sr2—O2^{vi}	85.67 (18)	Fe3^{iv}—O4—Sr1^{xvi}	122.2 (2)
O5^{ii}—Sr2—O2^{vi}	142.41 (18)	Fe4—O4—Sr2^{ix}	87.81 (19)
O3^{v}—Sr2—O2^{vi}	129.21 (18)	V3^{iv}—O4—Sr2^{ix}	103.8 (2)
O8—Sr2—O6^{vii}	175.50 (17)	Fe3^{iv}—O4—Sr2^{ix}	103.8 (2)
O5^{ii}—Sr2—O6^{vii}	80.68 (15)	Sr1^{xvi}—O4—Sr2^{ix}	95.86 (17)
O3^{v}—Sr2—O6^{vii}	96.47 (15)	Fe4—O5—V1^{xvii}	111.1 (3)
O2^{vi}—Sr2—O6^{vii}	97.91 (16)	Fe4—O5—Fe1^{xvii}	111.1 (3)
O8—Sr2—O4^{vi}	111.49 (16)	V1^{xvii}—O5—Fe1^{xvii}	0.00 (8)
O5^{ii}—Sr2—O4^{vi}	84.97 (15)	Fe4—O5—Sr2^{xvi}	124.3 (2)
O3^{v}—Sr2—O4^{vi}	164.10 (15)	V1^{xvii}—O5—Sr2^{xvi}	108.0 (2)
O2^{vi}—Sr2—O4^{vi}	60.41 (16)	Fe1^{xvii}—O5—Sr2^{xvi}	108.0 (2)
O6^{vii}—Sr2—O4^{vi}	68.34 (14)	Fe4—O5—Sr1^{xvii}	90.66 (18)
O8—Sr2—O7^{iv}	75.56 (16)	V1^{xvii}—O5—Sr1^{xvii}	90.07 (17)
O5^{ii}—Sr2—O7^{iv}	155.43 (15)	Fe1^{xvii}—O5—Sr1^{xvii}	90.07 (17)
O3^{v}—Sr2—O7^{iv}	68.68 (15)	Sr2^{xvi}—O5—Sr1^{xvii}	127.46 (19)
O2^{vi}—Sr2—O7^{iv}	60.55 (17)	V2^{xviii}—O6—Fe2^{xviii}	0.00 (9)
O6^{vii}—Sr2—O7^{iv}	108.56 (14)	V2^{xviii}—O6—Fe3	109.4 (2)
O4^{vi}—Sr2—O7^{iv}	119.55 (14)	Fe2^{xviii}—O6—Fe3	109.4 (2)
O1^{viii}—Fe1—O8^{ix}	107.2 (2)	V2^{xviii}—O6—Sr1^{iv}	112.6 (2)
O1^{viii}—Fe1—O5^{iii}	106.0 (2)	Fe2^{xviii}—O6—Sr1^{iv}	112.6 (2)
O8^{ix}—Fe1—O5^{iii}	108.2 (2)	Fe3—O6—Sr1^{iv}	121.7 (2)
O1^{viii}—Fe1—O3	111.0 (2)	V2^{xviii}—O6—Sr2^{xix}	100.9 (2)
O8^{ix}—Fe1—O3	120.2 (2)	Fe2^{xviii}—O6—Sr2^{xix}	100.9 (2)
O5^{iii}—Fe1—O3	103.4 (2)	Fe3—O6—Sr2^{xix}	108.6 (2)
O7^{x}—Fe2—O2	103.2 (2)	Sr1^{iv}—O6—Sr2^{xix}	101.25 (16)
O7^{x}—Fe2—O3	114.2 (2)	V2^{x}—O7—Fe2^{x}	0.00 (7)
O2—Fe2—O3	101.0 (2)	V2^{x}—O7—Fe4	119.6 (3)
O7^{x}—Fe2—O6^{xi}	109.0 (2)	Fe2^{x}—O7—Fe4	119.6 (3)
O2—Fe2—O6^{xi}	116.4 (2)	V2^{x}—O7—Sr1^{xvii}	137.4 (2)
O3—Fe2—O6^{xi}	112.6 (2)	Fe2^{x}—O7—Sr1^{xvii}	137.4 (2)
O1^{xii}—Fe3—O4^{iv}	118.2 (2)	Fe4—O7—Sr1^{xvii}	100.9 (2)
O1^{xii}—Fe3—O8^{xiii}	105.8 (2)	V2^{x}—O7—Sr2^{iv}	88.8 (2)
O4^{iv}—Fe3—O8^{xiii}	105.6 (2)	Fe2^{x}—O7—Sr2^{iv}	88.8 (2)
O1^{xii}—Fe3—O6	98.2 (2)	Fe4—O7—Sr2^{iv}	101.6 (2)
O4^{iv}—Fe3—O6	112.6 (2)	Sr1^{xvii}—O7—Sr2^{iv}	95.81 (17)

O8^{xiii}—Fe3—O6	116.8 (2)	V1^{vi}—O8—Fe1^{vi}	0.00 (10)
O4—Fe4—O2	99.6 (2)	V1^{vi}—O8—V3^{viii}	108.4 (2)
O4—Fe4—O7	111.1 (2)	Fe1^{vi}—O8—V3^{viii}	108.4 (2)
O2—Fe4—O7	110.2 (3)	V1^{vi}—O8—Fe3^{viii}	108.4 (2)
O4—Fe4—O5	114.8 (2)	Fe1^{vi}—O8—Fe3^{viii}	108.4 (2)
O2—Fe4—O5	119.9 (2)	V3^{viii}—O8—Fe3^{viii}	0.00 (6)
O7—Fe4—O5	101.5 (2)	V1^{vi}—O8—Sr2	126.4 (2)
V1^{xiii}—O1—Fe1^{xiii}	0.00 (6)	Fe1^{vi}—O8—Sr2	126.4 (2)
V1^{xiii}—O1—V3^{xii}	126.0 (3)	V3^{viii}—O8—Sr2	123.1 (2)
Fe1^{xiii}—O1—V3^{xii}	126.0 (3)	Fe3^{viii}—O8—Sr2	123.1 (2)

Symmetry codes: (i) $x+1/2, -y+1/2, z-1/2$; (ii) $-x+3/2, y+1/2, -z+1/2$; (iii) $x-1/2, -y+1/2, z-1/2$; (iv) $-x+1, -y+1, -z+1$; (v) $-x+1/2, y+1/2, -z+1/2$; (vi) $x, y+1, z$; (vii) $x+1/2, -y+3/2, z-1/2$; (viii) $x, y, z-1$; (ix) $x, y-1, z$; (x) $-x+1, -y, -z+1$; (xi) $-x+1/2, y-1/2, -z+3/2$; (xii) $-x, -y+1, -z+2$; (xiii) $x, y, z+1$; (xiv) $x-1/2, -y+1/2, z+1/2$; (xv) $-x+1/2, y-1/2, -z+1/2$; (xvi) $-x+3/2, y-1/2, -z+1/2$; (xvii) $x+1/2, -y+1/2, z+1/2$; (xviii) $-x+1/2, y+1/2, -z+3/2$; (xix) $x-1/2, -y+3/2, z+1/2$.